Integrated multi-wavelength microscope combining TIRFM and IRM modalities for imaging cellulases and other processive enzymes

Daguan Nong,[1] Zachary K. Haviland,[1] Kate Vasquez Kuntz,[2] Ming Tien,[3] Charles T. Anderson,[2] ⊙ **and William O. Hancock[1],*** ⊙

[1]*Department of Biomedical Engineering, Pennsylvania State University, University Park, PA 16802, USA*
[2]*Department of Biology, Pennsylvania State University, University Park, PA 16802, USA*
[3]*Department of Biochemistry and Molecular Biology, Pennsylvania State University, University Park, PA 16802, USA*
*woh1@psu.edu

Abstract: We describe a multimodal microscope for visualizing processive enzymes moving on immobilized substrates. The instrument combines interference reflection microscopy (IRM) with multi-wavelength total internal reflectance fluorescence microscopy (TIRFM). The microscope can localize quantum dots with a precision of 2.8 nm at 100 frames/s, and was used to image the dynamics of the cellulase, Cel7a interacting with surface-immobilized cellulose. The instrument, which was built with off-the-shelf components and is controlled by custom software, is suitable for tracking other degradative enzymes such as collagenases, as well as motor proteins moving along immobilized tracks.

1. Introduction

Cellulases, collagenases, and ribonucleases are all examples of processive enzymes that catalyze the degradation of their biopolymer substrates [1–3]. Mechanistic understanding of these enzymes requires simultaneously imaging individual enzyme molecules and the substrate on which they are acting. Particle tracking by TIRFM has been used extensively to study motor proteins moving along cytoskeletal tracks [4]. These approaches generally require using different fluorophores to separately localize the motors and the tracks. By exciting fluorophores with an evanescent wave generated by total internal reflection, only fluorophores within ~100 nm of the glass surface are excited, which minimizes background fluorescence and generates high signal-to-noise ratios for single-molecule imaging. By fitting the point spread function of spatially isolated motor proteins, localization down to nanometer spatial precision can be achieved using this approach [5]. This tracking precision is aided by actin filaments or microtubules being easy to polymerize *in vitro* and disperse, which ensures that motors are moving along single, isolated tracks.

Observing enzymes on more complex substrates such as collagen and cellulose is hindered by the branched network structures of the substrates, which also have thicknesses that can extend beyond the evanescent field of TIRFM. Furthermore, if both the enzyme and the substrate on which it is acting are fluorescently labeled, crosstalk between fluorescence channels can occur, limiting localization precision. One solution to this problem is to use different imaging modalities for the mobile enzyme and the surface-immobilized substrate. In the last decade, Interferometric Scattering Microscopy (iSCAT) and IRM have been used to image unlabeled actin filaments and microtubules [6–14]. These techniques rely on interference between scattered photons from the sample and reflection at the glass-water interface [6]. They offer high signal-to-noise ratios and, because of the large number of reflected photons, allow for imaging at kHz frame rates [9,15].

Here, we report the construction and application of a new microscope that integrates IRM with multi-wavelength TIRFM. The system is built around an open construction, commercially available microscopy platform and uses off-the-shelf components. Specific features include both micromirror- and dichroic-based total internal reflectance (TIR) excitation; six lasers that are co-aligned for simultaneous excitation in micromirror mode; integration of the IRM into the dichroic illumination pathway; real-time axial drift correction that stabilizes focus to within 25 nm; and localization precision of 2.8 nm for quantum dots at 100 frames/s. Control of lasers, shutters, and the piezo-stage, as well as image acquisition by the camera are accomplished by a custom LabVIEW software package that is freely available. As a proof of concept, we used the microscope to image the binding and processive movement of the cellulase Cel7A from *Trichoderma reesei* on bacterial cellulose. The system is flexible and can be adapted for a wide range of biological applications where high-resolution, simultaneous tracking of motile proteins and imaging of complex substrates is needed.

2. Methods

2.1. Microscope design and assembly

The microscope combines objective-based TIRFM through both micromirror and dichroic mirror pathways, together with dichroic-based epifluorescence and IRM (Fig. 1). The instrument is built on an optical table around a Mad City Labs RM21 platform, with samples mounted atop a three-axis piezoelectric translation stage ($200 \times 200 \times 200$ µm, Nano-LPS200, Mad City Labs; USA). Illumination is provided by six lasers (Oxxius; France): LBX-405-180-CSB-PPA (405 nm, 180 mW), LBX-488-150-CSB-PPA (488 nm, 150 mW), LCX-532L-100-CSB-PPA (532 nm, 100 mW), LCX-561L-100-CSB-PPA (561 nm, 100 mW), LBX-647-140-CSB-PPA (647 nm, 140 mW), LBX-785-100-CSB-PPA (785 nm, 50 mW). Each laser beam travels through a f = 25 mm focusing lens (Lf, AL2520-A, Thorlabs; USA), a 25 µm pinhole (Ph, P25 Da, Thorlabs; USA), and a f = 250 mm expanding lens (Le, LA1461-A-ML, Thorlabs; USA) to yield a clean and 10-fold expanded beam. Irises (Ir, SM1D12C, Thorlabs; USA) are used to adjust the beam size after expansion. The expanded beams are combined using five dichroic mirrors (T760lpxr, DM1; T590lpxr, DM2; T545lpxr, DM3; T510lpxr, DM4; T470lpxr, DM5; Chroma, USA) and a broadband mirror, which are all mounted on kinematic mirror mounts (KCB1C/M, Thorlabs; USA) to achieve a co-aligned beam.

The microscope includes two illumination pathways, micromirror and dichroic, that can be switched using a flip mirror (M1; FM90, Thorlabs; USA). In the micromirror pathway, the beam is raised by a periscope and then passes through a focusing lens (L1, f = 150 mm) mounted on an x-y translation stage (CXY1, Thorlabs; USA). By adjusting the x-y position of L1, the beam is centered onto a 2.8-mm ellipsoidal mirror, hereafter termed micromirror (MM1, G54-092, Edmund Optics; USA), which is positioned close (< 2 mm) to the back of the objective (APON 60XOTIRF, NA = 1.49, Olympus; Japan). Following total internal reflection at the glass-water interface of the sample, the beam returns through the objective and is reflected by a second micromirror (MM2, G54-092, Edmund Optics; USA), passes through a focusing lens (L2, f = 150 mm) and a bandpass fiter (F1, et775-50x, Chroma; USA), and arrives at a quadrant photodiode (QPD; TIRF Lock, Mad City Labs; USA). Micromirrors MM1 and MM2 are separately mounted on translation stages (T12X, Thorlabs; USA) and are manually adjusted to achieve the optimal TIR illumination angle. The QPD is placed approximately 300 mm from L2 in a slightly defocused position to achieve optimal sensitivity. The position of this exit beam on the QPD varies with the distance between the objective lens and the sample, and is used for z-drift correction by the piezo stage.

In the dichroic illumination pathway, the beam is first raised by a periscope, reflected by a pair of mirrors (M3 and M4), passed through a focusing lens (L3, f=150 mm), and reflected off a dichroic mirror (DM6, ZET488/640m-TRF, Chroma; USA) placed under the objective.
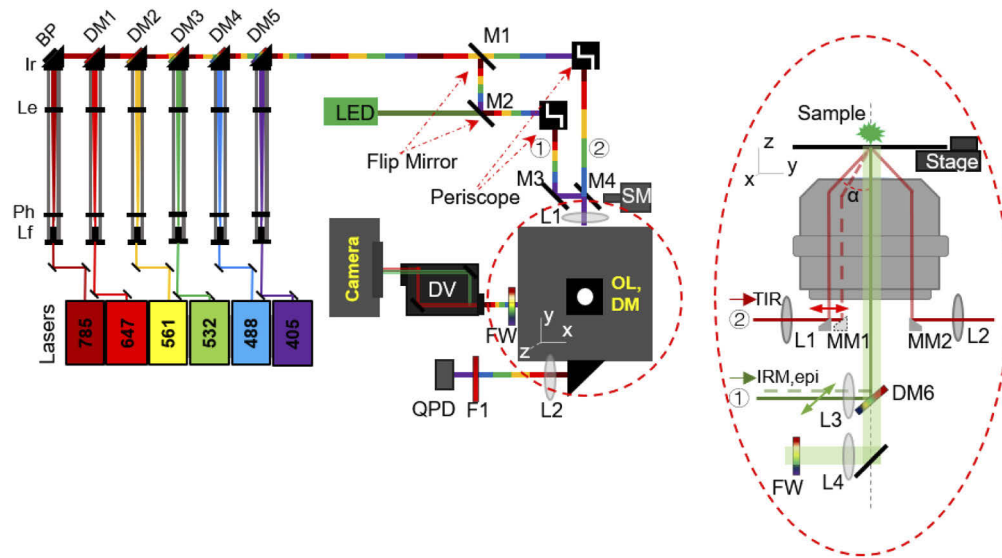
Fig. 1. Microscope schematic. Illumination is provided by six lasers at left that are each expanded and collimated by a pair of lenses (Lf and Le) and a pinhole (Ph), Irises (Ir) are used to adjust the beam size after expansion. The beams are combined and collimated by a series of dichroic mirrors (DM1-DM5). The 785 nm beam used for auto-focus is reflected off of a broadband mirror (BP). This combined illumination beam is used for dichroic-based illumination (1) or micromirror-based illumination (2), depending on the position of flip mirrors M1 and M2. In the dichroic pathway, the position of mirrors M3 and M4 are adjusted to switch between TIRFM and epi-fluorescence modes. IRM illumination is supplied by an LED that is reflected off a dichroic mirror below the objective. Images pass through a filter wheel (FW) and dual-view system (DV) before being captured by the camera. Auto-focus is achived using a quadrant photodiode downstream of a bandpass filter (F1) and lens (L2). At right is a detailed view of the objective and associated components, showing micromirrors (MM1 and MM2) for TIR excitation in the back of the objective, and the dichroic mirror (DM6) used for both IRM and dichroic-based TIRFM or epi-fluorescence illumination. Note that only the lenses (L1 and L2) used for micromirror TIR excitation are shown in figure at left; lenses for all beam paths are shown at right. See text for full description of components.

M3 is mounted on a kinematic mirror mount (KS1 T, Thorlabs; USA) and M4 is mounted on a translatable stage driven by a stepper motor (SM, Mad City Labs; USA). Translating M4 horizontally results in a corresponding translation of the excitation beam in the back focal plane of the objective, thus enabling switching between epifluorescence and TIR illumination modes.

The IRM illumination pathway uses a green LED (525 nm, 130 mW; Thorlabs; USA) that is co-aligned with the laser beam before being reflected off the dichroic mirror. Switching between IRM and epi/TIR modes is accomplished by a flip mirror (M2; FM90, Thorlabs; USA). With this design, simultaneous IRM and TIRFM is achieved using the micromirror TIR pathway.

In the imaging pathway, emitted photons collected by the objective first pass through the dichroic mirror (DM6), then through a f = 500 mm focusing lens (L4). Fluorescence emission wavelengths are selected by a filter wheel (CFW6, Thorlabs; USA) and a dual-view system (OptoSplit II, Photometrics; USA) before being focused into the camera (Prime 95B, Photometrics; USA).

2.2. Software workflow

All hardware and image acquisition systems are controlled by custom-designed software implemented in LabVIEW in Actor Framework (LabVIEW 2019, National Instruments; Austin, TX). The workflow of the main Virtual Instrument is illustrated in Fig. 2. The software was designed to serve as a flexible platform for microscope control that can support different hardware modules and be easily modified to add new extensions based on future imaging needs. The software was designed with four different layers, as follows. 1) The Hardware Layer handles communication to specific hardware components. 2) The Hardware Abstraction Layer serves as an interface between the hardware and logic layers, and carries out the common functional calls to the hardware (e.g., obtain and set stage position or laser power; set camera exposure and acquire image sequence). 3) The Logic Layer defines the specific microscope modality and defines specific functions (e.g., switching lasers in a defined sequence). The Logic Layer was designed to communicate directly with the Hardware Extraction Layer and operate without regard to the specific hardware components present. 4) The User Interface Layer controls the Logic Layer and enables the user to control all aspects of the microscope.

Following an object-oriented programing approach, base Actor classes were defined to control common hardware elements such as the stage, laser, and camera. Under this framework, hardware components of a similar class are interchangeable. To install new components, such as a new camera, a new Actor derived from the base Actor class is created to directly communicate with the specific hardware component. This strategy minimizes the requirement for new coding when hardware is replaced or upgraded, or if the software is used with a different microscope. In our microscope, a Camera_Prime95B actor was derived from the Camera base class to control the camera, a Stage_MadCityLab actor was derived from the Stage base class to control the stage, and a Laser_Oxxius actor was derived from the Laser base class to control the laser (Fig. 2). A TIR_Lock actor, derived from the Analyser, was created to maintain focus by reading the QPD voltage, comparing it to the lock target voltage, and using a proportional/integrative controller to move the stage. Images, movies, and hardware status information were handled by the DataCollector actor and saved for further analysis. The latest version of the software is available on Github (https://github.com/erisir/MMicroscopy.git).

2.3. Cellulose and cellulase preparation and imaging

Acetobacter cellulose was purified from *G. hansenii* (strain ATCC 23769), washed with 100% ethanol, and incubated with 2% (w/v) NaOH for 30 min at 80 °C. The cellulose was then centrifuged for 15 min at 2300xg, resuspended in 0.5 M NaOAc to neutralize it, and centrifugation repeated twice more with resuspension in sterile ddH$_2$O. The cellulose was then air dried for 2 days, followed by resuspension and sonication. The sonicated sample was passed five times through a 200 μm filter, once through a 75 μm filter, and processed through a M-110EH microfluidizer (Microfluidics International, Westwood, MA, USA). Cel7a from *Trichoderma reesei* (Sigma E6412) and microbial Cel6a (Megazyme E-CBHIIM) were biotinylated using biotin-NHS (Thermo Scientific, catalog number: 21343). Flow chambers for microscopy were assembled by sandwiching a piece of double-sided tape between a slide and a plasma-cleaned coverslip (Fisherbrand; USA). A sample consisting of 20 μL of ~3 mg/mL cellulose was pipetted into the flow cell and the slide was allowed to dry at 80 °C for 5 min until the cellulose fibers were adhered to the coverslip surface. Twenty microliters of a 1:200 dilution of tetraspeck beads (four excitation/emission peaks of 356/430 nm, 505/515 nm, 560/580 nm, and 660/680 nm; Thermo Scientific) was flowed in and incubated for 5 min. This tetraspeck dilution was chosen empirically to achieve approximately 5-10 beads per field of view. Next, the flow cell was flushed three times with 20 μL of 1 mg/mL bovine serum albumin (BSA, EMD Millipore) and incubated for 5 min to block the surface from nonspecific interactions. Cellulose fibers were located using IRM and, after fine-focus adjustments, the TIR-Lock system was engaged to keep the sample in focus.
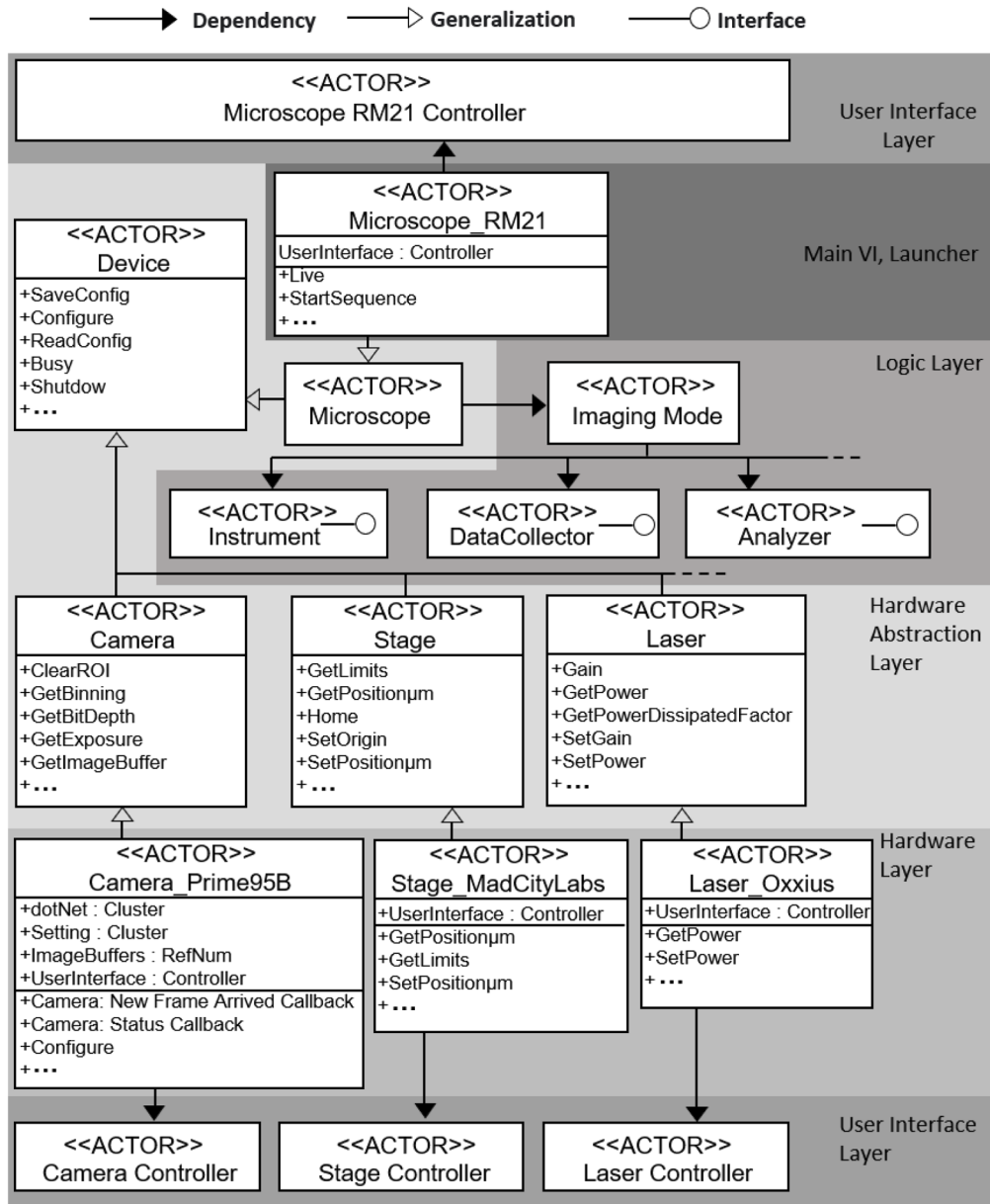
Fig. 2. Software workflow for controlling the microscope. See text for details.

Finally, a 20 µL solution containing 2 nM Cel7a labeled with Qdot525 and/or Cel6A labeled with Qdot655 in 50 mM NaOAc and 5 mM dithiothreitol, pH 5.0 was flowed in. The illumination was changed to micromirror TIRFM mode with 405 nm excitation at 100 mW, and 500 frame movies enzymes interacting with the immobilized cellulose were captured at 10 frames/s using 63 ms exposures. At the end of each acquision, simultaneous micromirror TIRFM and IRM images were taken for colocalizing enzymes with cellulose substrate.

3. Results and discussion

3.1. TIR-lock performance

To prevent the sample from drifting out of focus during long data collection periods, a closed-loop focus feedback system was implemented. A constant distance between the sample and the objective lens was maintained by monitoring the QPD voltage and moving the piezo-stage to minimize voltage changes (Fig. 3(a)). The auto-focus system was calibrated by stepping the stage in known increments and recording the QPD output voltage to create a calibration curve (2.26 V/µm; Fig. 3(b)). Based on this calibration, the z-position of the stage was controlled in the software proportional-integral control loop. The stability of system was checked by manually applying a sample displacement of ~1 µm and observing the system response (Fig. 3(c)). Upon stage displacement, the QPD voltage in the y-direction dropped immediately, while voltage in the x-direction remained constant as expected (Fig. 3(c), upper panel). The z-position of the stage was moved in response (Fig. 3(c), bottom panel) until the QPD voltage returned to its target. After TIR-lock was established, the standard deviation of the QPD signal in the y-direction was 0.055 V, demonstrating that the system was able to maintain focus with a precision of ± 24 nm.

3.2. Qdot tracking

To track Qdots, we used micromirror TIR, which minimizes signal loss by dichroic mirrors and facilitates multi-wavelength excitation. Figure 4(a) depicts a high-constrast quantum dot image (Qdot525, Thermo Scientific, catalog number: Q10143MP), achieved using micromirror excitation by a 405 nm laser.

The position of the Qdot was fitted using FIESTA image analysis software [16], which uses Gaussian fitting of the point spread function to achieve sub-pixel positional precision (Fig. 4(a)). To convert pixel size to nm in FIESTA, we measured pixel size by moving the piezoelectric stage in known increments. Figure 4(b) shows that the line of best fit has a slope of 15.1 pixels/µm (66.2 nm/pixel) in the x- and y-directions. This value agreed well with our theoretical calculation of 65.98 nm/pixel, calculated by dividing the camera pixel size (11 µm) by the estimated total magnification of the microscope (166.7x).

We tested the tracking precision of our system by comparing measured step-wise displacements of an immobilized Qdot525 to programmed step-wise displacements of the piezoelectric stage. The Qdot525 displacements closely matched the stage displacements, and the standard deviation of the plateau regions was 2.8 nm at a frame rate of 100 Hz (5 ms exposure, 405 nm excitation at 150 mW) (Fig. 4(c)). Thus, we define the current tracking precision of the microscope to be 2.8 nm at 100 frames/s. By analyzing particle positions using a 10-frame boxcar average, the standard deviation of position calculations improved to 0.87 nm (Fig. 4(c)).

3.3. Simultaneous imaging of Cel7a enzyme and cellulose substrate

Co-imaging processive enzymes and their substrates is crucial for revealing the biological mechanisms of these enzymes. A common method of imaging cellulose is fluorescence microscopy using the cellulose-binding dye Pontamine Fast Scarlet 4B (S4B) or the glucan-binding dye Calcofluor White [17]. However, these dyes can be excited over and emit over broad wavelength ranges, which introduces crosstalk into other fluorescence channels. This
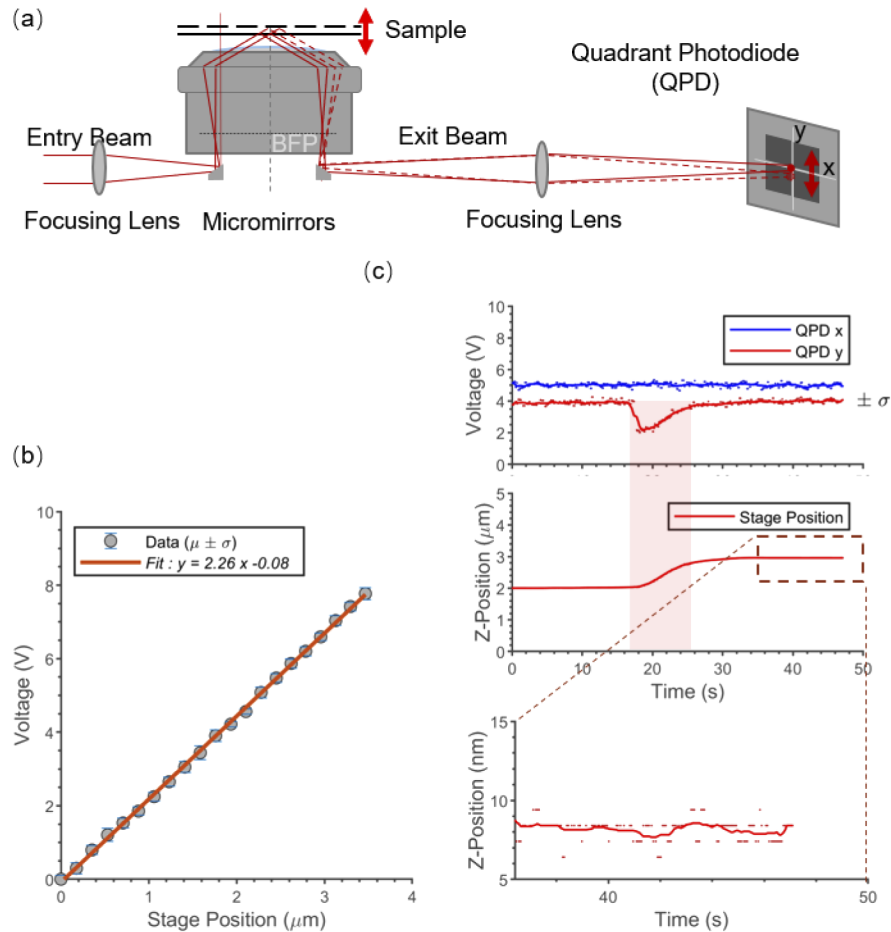
Fig. 3. TIR-lock system. a) Schematic showing how changes in sample height above the objective were detected. An infrared beam (785 nm) collimated with the excitation lasers was totally internally reflected from the glass-water interface of the sample and focused onto the QPD. Changes in sample height caused displacements of the beam that were detected by the QPD. b) Calibration curve of QPD voltage for different z-positions of the stage. c) Step response of the closed-loop feedback system to a ~1 μm manual step change in the stage height. QPD voltages (top) for vertical (y) and horizontal (x) directions, and stage z-position in μm (middle) and nm (bottom).
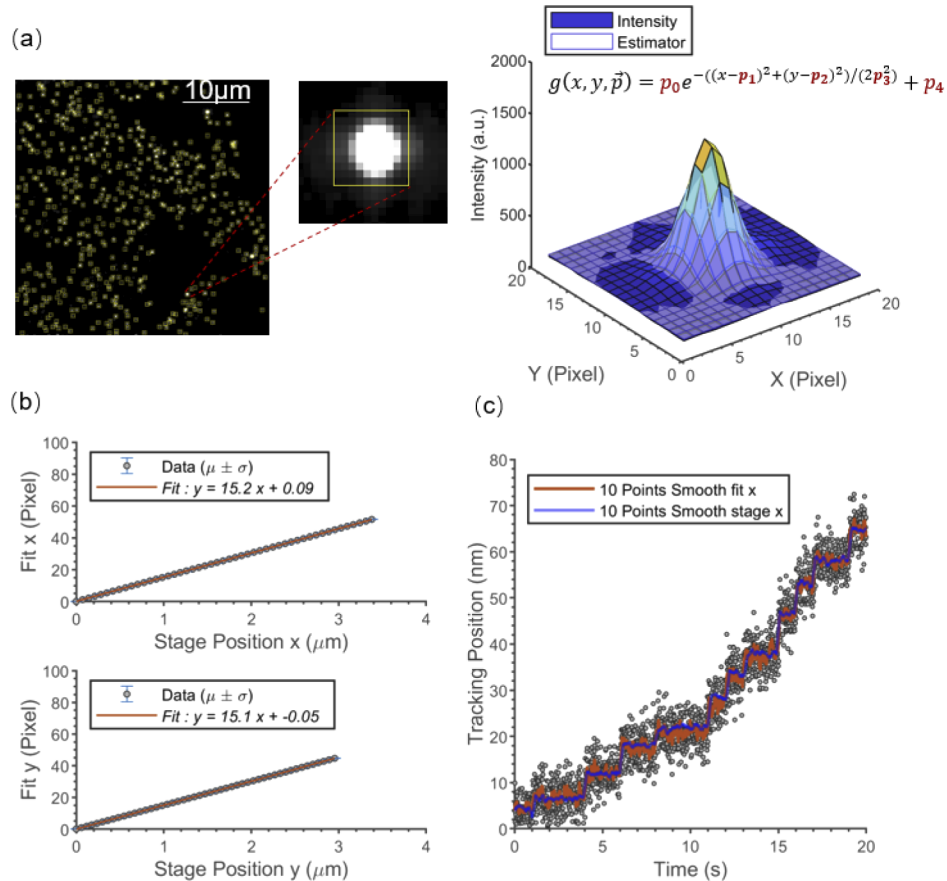
Fig. 4. High-resolution tracking of Qdot positions. a) Raw images of Qdot-labeled Cel7a bound to immobilized cellulose (left, with zoomed region middle); image intensity profile of a single Qdot (right). b) Calibration curve to measure pixel size in x (top) and y (bottom). c) Trace of a surface-immobilized Qdot moving due to programmed step changes in stage position. Images were taken at 100 frames/s in a 30 by 30 pixel region of interest. The stage was stepped in random increments between 0 and 20 nm (blue curve), and the Qdot position was calculated by point-spread-function fitting. Gray points are raw position data and the red curve is data smoothed with a 10-point boxcar average. The standard deviation at each step is 2.8 nm for the raw data and 0.87 nm for the 10-point boxcar.

crosstalk can degrade tracking accuracy for the enzymes, and the presence of dye molecules on the cellulose surface might interfere with enzyme binding and/or hydrolysis. To achieve label-free imaging of cellulose, we integrated IRM into our multi-wavelength TIRFM microscope using a separate imaging pathway. Typically, IRM uses a 50/50 beam splitter in the dichroic position of the standard epifluorescence illumination pathway [18,19]. Instead, we introduced a separate LED illumination source into the dichroic illumination pathway (Fig. 1). In this configuration, the shared dichroic mirror (Fig. 1; DM6) serves as a ~2:98 beam splitter in the IRM pathway, with ~2% reflection and 98% transmission for the 525 nm LED. This arrangement maximizes transmission in the TIRFM channel while maintaining high contrast in the IRM image.

To demonstrate the utility of IRM for imaging cellulose, we compared the intensity profile of an IRM image of label-free cellulose to an intensity profile of TIRFM imaging of the same cellulose after staining with S4B dye. Cellulose was adsorbed to a coverslip and imaged with IRM (50 ms exposure at 20 mW LED power; Fig. 5(a), left). The sample was then moved 40 μm out of focus, and a defocused image was taken and used to normalize for any illumination inhomogeneities across the sample field. Next, 0.5% (w/v) S4B in 50 mM NaOAc, pH 5.0 was introduced into the sample chamber, incubated for 5 min to allow for dye binding, and washed out of the flow cell with 200 μL of 50 mM NaOAc, pH 5.0. Finally, images of the same field were captured by TIRFM (Fig. 5(a), right; 405 nm excitation with 463 ms exposure at 100 mW laser power). As shown in Fig. 5(b), the signal intensity profile of IRM was comparable to the TIRFM signal.
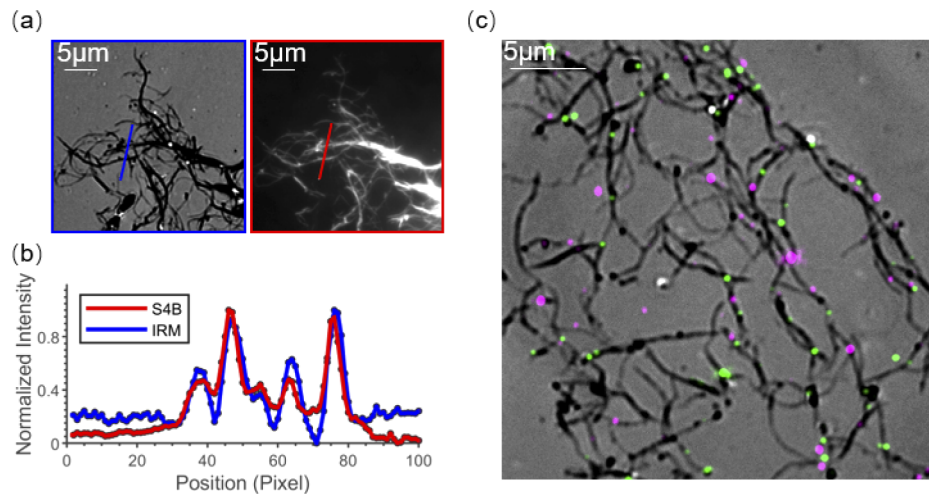

Fig. 5. Simultaneous imaging of cellulases and cellulose. a) IRM images of label-free cellulose (left) and TIRFM images of S4B labeled cellulose (right) in the same region. b) Intensity profile comparison of IRM (blue line) and TIRFM (red line). The IRM image intensity was inverted and scaled to show overlap with fluorescence. c) Composite image of immobilized cellulose imaged by IRM (black fibers on the gray background) with Qdot525-labeled-Cel7a (Green) and Qdot655-labeled Cel6a (Magenta) imaged by two-color micromirror TIRFM.

To test the microscope's ability to combine two-color TIRFM with IRM, we acquired movies of Qdot525-labeled Cel7a and Qdot655-labeled Cel6a interacting with unlabeled cellulose at 2 frame/s (463 ms exposure, 405 nm excitation, laser power 100 mW) in micromirror TIRFM. An IRM movie was then acquired to confirm colocalization of the Qdot-labeled enzymes with the immobilized substrate. Figure 5(c) shows Qdot525-Cel7a (green) and Qdot655-Cel6a (magenta) bound to the unlabeled cellulose fibers (black fibers on the gray background) with high

colocalization precision, confirming that the system can be used to image label-free substrate along with simultaneous imaging of two different enzyme populations.

3.4. Imaging movement of Cel7a cellulase along immobilized cellulose

To demonstrate a practical application of the hybrid IRM-TIRFM microscope, we imaged Qdot525-labeled-Cel7a moving along immobilized cellulose (Fig. 6). Image stacks were analyzed by FIESTA software [16] to obtain sub-pixel localization of the Qdots. The kinetic behaviors of the molecules were then analyzed and categorized with our custom Matlab software [20] (available on Github at https://github.com/erisir/SingleParticleTracking.git). Simultaneous imaging of the enzyme and the track is shown in Fig. 6(a), the movement of one enzyme in x-y is shown in Fig. 6(b), and the displacement versus time is shown in Fig. 6(c). The Cel7a molecule moves processively and pauses intermittently. In a related study [20], we used this system to analyze 11,116 Cel7a trajectories and categorized their diverse behaviors.
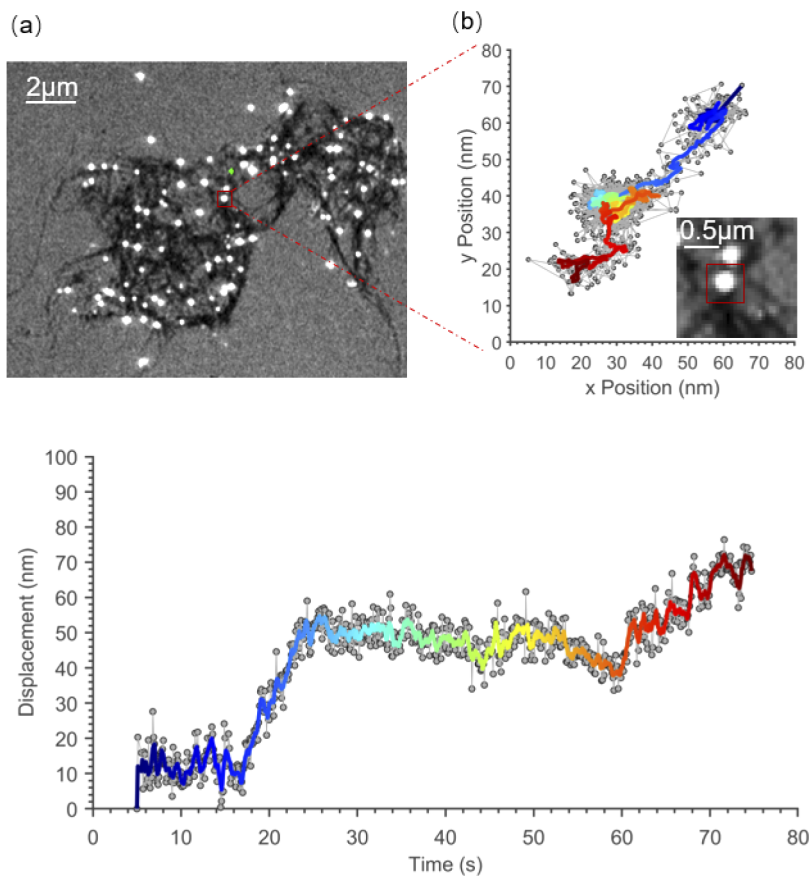

Fig. 6. High-resolution tracking Cel7a on cellulose. a) Simultaneous imaging of cellulose (black fibers on the gray background) and Qdot525-labeled-Cel7a (bright spots). b) x-y plot of Qdot position, showing Cel7a moving unidirectionally along the cellulose. Gray points are raw data and color curve is data smoothed with a 5-point boxcar. Time is coded by color, from blue to red. c) Displacement from the origin versus time from the same data. Gray points are raw data at 10 fps sampling rate and color curve is data smoothed with a 5-point boxcar, showing the Qdot-labeled Cel7a moving processively along the cellulose with intermittent pauses.

4.   Conclusion

We developed new capabilities for imaging processive enzymes on heterogeneous substrates by integrating IRM with multi-wavelength TIRFM into a multimodal microscope and developed companion software to control the hardware and image acquisition. Using a closed-loop feedback system, the instrument can stabilize the sample focus within 25 nm. Using micro-mirror TIRFM, the system can track Qdots at 100 frames/s with a minimum positional precision of 2.8 nm. Micromirror TIRFM has been shown to be efficient at multi-wavelength excitation experiments [21], and here we demonstrate that with careful choice of laser lines and filters, two color imaging is relatively simple. We find that IRM enables label-free imaging of branched networks of cellulose that extend beyond the evanescent field. We validated the capabilities of the instrument by imaging fluorescent Cel7a enzymes interacting with immobilized cellulose. The instrument has a flexible architecture that also has the capability to expand to interferometric scattering (iSCAT) and stochastic optical reconstruction (STORM) microscopy, and these approaches can be applied together to study other processive enzyme-substrate systems such as cytoskeletal motors.

References

1.   K. Igarashi, T. Uchihashi, A. Koivula, M. Wada, S. Kimura, T. Okamoto, M. Penttilä, T. Ando, and M. Samejima, "Traffic jams reduce hydrolytic efficiency of cellulase on cellulose surface," Science **333**(6047), 1279–1282 (2011).
2.   S. Saffarian, I. E. Collier, B. L. Marmer, E. L. Elson, and G. Goldberg, "Interstitial collagenase is a Brownian ratchet driven by proteolysis of collagen," Science **306**(5693), 108–111 (2004).
3.   N. G. Nossal and M. F. Singer, "The processive degradation of individual polyribonucleotide chains: I. Escherichia coli ribonuclease II," J. Biol. Chem. **243**(5), 913–922 (1968).
4.   A. Yildiz, M. Tomishige, R. D. Vale, and P. R. Selvin, "Kinesin walks hand-over-hand," Science **303**(5658), 676–678 (2004).
5.   A. Yildiz, J. N. Forkey, S. A. McKinney, T. Ha, Y. E. Goldman, and P. R. Selvin, "Myosin V walks hand-over-hand: single fluorophore imaging with 1.5-nm localization," Science **300**(5628), 2061–2065 (2003).
6.   J. Ortega-Arroyo and P. Kukura, "Interferometric scattering microscopy (iSCAT): new frontiers in ultrafast and ultrasensitive optical microscopy," Phys. Chem. Chem. Phys. **14**(45), 15625–15636 (2012).
7.   J. Andrecka, J. O. Arroyo, K. Lewis, R. A. Cross, and P. Kukura, "Label-free imaging of microtubules with sub-nm precision using interferometric scattering microscopy," Biophys. J. **110**(1), 214–217 (2016).
8.   J. Ortega Arroyo, J. Andrecka, K. Spillane, N. Billington, Y. Takagi, J. Sellers, and P. Kukura, "Label-free, all-optical detection, imaging, and tracking of a single protein," Nano Lett. **14**(4), 2065–2070 (2014).
9.   K. J. Mickolajczyk, N. C. Deffenbaugh, J. Ortega Arroyo, J. Andrecka, P. Kukura, and W. O. Hancock, "Kinetics of nucleotide-dependent structural transitions in the kinesin-1 hydrolysis cycle," Proc. Natl. Acad. Sci. **112**(52), E7186–E7193 (2015).
10. K. J. Mickolajczyk, E. A. Geyer, T. Kim, L. M. Rice, and W. O. Hancock, "Direct observation of individual tubulin dimers binding to growing microtubules," Proc. Natl. Acad. Sci. **116**(15), 7314–7322 (2019).
11. M. Mahamdeh, S. Simmert, A. Luchniak, E. Schäffer, and J. Howard, "Label-free high-speed wide-field imaging of single microtubules using interference reflection microscopy," J. Microsc. **272**(1), 60–66 (2018).
12. M. Abercrombie and G. A. Dunn, "Adhesions of fibroblasts to substratum during contact inhibition observed by interference reflection microscopy," Exp. Cell Res. **92**(1), 57–62 (1975).
13. E. Au, "Optical tweezers and multimodality imaging: a platform for dynamic single-molecule analysis," Biophys. J. **118**(3), 620a (2020).
14. S. Simmert, M. K. Abdosamadi, G. Hermsdorf, and E. Schäffer, "LED-based interference-reflection microscopy combined with optical tweezers for quantitative three-dimensional microtubule imaging," Opt. Express **26**(11), 14499–14513 (2018).
15. K. M. Spillane, J. Ortega-Arroyo, G. de Wit, C. Eggeling, H. Ewers, M. I. Wallace, and P. Kukura, "High-speed single-particle tracking of GM1 in model membranes reveals anomalous diffusion due to interleaflet coupling and molecular pinning," Nano Lett. **14**(9), 5390–5397 (2014).

16. F. Ruhnow, D. Zwicker, and S. Diez, "Tracking single particles and elongated filaments with nanometer precision," Biophys. J. **100**(11), 2820–2828 (2011).

17. C. T. Anderson, A. Carroll, L. Akhmetova, and C. Somerville, "Real-time imaging of cellulose reorientation during cell wall expansion in Arabidopsis roots," Plant Physiol. **152**(2), 787–796 (2010).

18. A. Curtis, "The mechanism of adhesion of cells to glass: a study by interference reflection microscopy," J. Cell Biol. **20**(2), 199–215 (1964).

19. H. Verschueren, "Interference reflection microscopy in cell biology: methodology and applications," J. Cell Sci. **75**(1), 279–301 (1985).

20. Z. K. Haviland, D. Nong, K. V. Kuntz, T. J. Starr, D. Ma, M. Tien, C. T. Anderson, and W. O. Hancock, "Nanoscale dynamics of cellulase TrCel7A digesting cellulose," bioRxiv (2021).

21. L. J. Friedman, J. Chung, and J. Gelles, "Viewing dynamic assembly of molecular complexes by multi-wavelength single-molecule fluorescence," Biophys. J. **91**(3), 1023–1031 (2006).

22. D. Nong, "Dataset 1," Scholarsphere (2021), https://doi.org/10.26207/0mnz-xj93